HHS Public Access

Author manuscript

Nat Methods. Author manuscript; available in PMC 2010 January 01.

Published in final edited form as:

Nat Methods. 2009 July ; 6(7): 532–537. doi:10.1038/nmeth.1341.

Mapping the structure and conformational movements of proteins with transition metal ion FRET

Justin W. Taraska[1], **Michael C. Puljung**[1], **Nelson B. Olivier**[2], **Galen E. Flynn**[1], and **William N. Zagotta**[1]

[1] Department of Physiology and Biophysics, Howard Hughes Medical Institute, University of, Washington, Seattle, Washington 98195

[2] Department of Chemistry, Massachusetts Institute of, Technology, Cambridge, Massachusetts 02139

SUMMARY

Visualizing conformational dynamics in proteins has been difficult, and the atomic-scale motions responsible for the behavior of most allosteric proteins are unknown. Here, we report that FRET between a small fluorescent dye and a nickel ion bound to a di-histidine motif can be used to monitor small structural rearrangements in proteins. This method provides several key advantages over classical FRET including the ability to measure the dynamics of close range interactions, the use of small probes with short linkers, a low orientation dependence, and the ability to add and remove unique tunable acceptors. We used this 'transition metal ion FRET' approach along with x-ray crystallography to determine the structural changes of the gating-ring of the mouse hyperpolarization-activated cyclic nucleotide-regulated ion channel HCN2. Binding of cAMP to the isolated carboxyl-terminal region of HCN2 caused a structural rearrangement involving a movement of the C-helix towards the β-roll of the cAMP-binding domain and a movement of the F′ helix of the C-linker, along with a stabilization of the secondary structure of the helices. Our results suggest a general model for the conformational switch in the cyclic nucleotide-binding site of cyclic nucleotide-regulated ion channels.

INTRODUCTION

In allosteric proteins, the binding of a ligand stabilizes conformational rearrangements, resulting in a switch between inactive and active states. These movements can propagate long distances to affect activity tens of angstroms from the ligand-binding site. In HCN channels, the direct binding of cAMP to a cytoplasmic ligand-binding domain stabilizes the opening conformational changes in the channel pore located more than 50 Å away1.

Address correspondence to: William N. Zagotta, Ph.D. Dept. of Physiology and Biophysics, Box 357290, University of Washington, Seattle, WA 98195-7290, Tel: (206) 685-3878, Fax: (206) 543-0934, zagotta@u.washington.edu.

AUTHOR CONTRIBUTIONS

J.W.T designed the experiments and analysis. J.W.T and M.C.P. performed fluorescence experiments. N.B.O, G.E.F, and W.N.Z, performed the crystallography. J.W.T and W.N.Z. wrote the manuscript.

However, like in most allosteric proteins, the direction, magnitude, and nature of conformational changes in the channel are unknown.

Fluorescence resonance energy transfer (FRET), in which light energy absorbed by a donor is transferred to a nearby acceptor, is a powerful tool for measuring changes in molecular distances2. The efficiency of FRET falls off with the sixth power of the distance between the two molecules, making FRET exquisitely sensitive to changes in distance. However, as a consequence of this steep distance dependence, FRET can measure distances effectively only in a narrow window around R_0, the distance at which FRET efficiency is 50%2. Classical FRET methods are not always well suited to study intramolecular movements in proteins. This is chiefly due to the long R_0 values of most fluorescent dye or protein FRET pairs (30–60 Å), their large sizes (15–30 Å), and their long flexible attachment linkers (10–15 Å) 3,4. Combined with the dependence of the FRET on the relative orientation of the fluorophores, these properties can complicate the interpretation of FRET results. While lanthanide resonance energy transfer (LRET) methods have less orientation dependence than FRET, LRET still utilizes large chelating groups and dyes with long linkers, has similarly long R_0 values (~30–100 Å), and has the added complication of very long excited state lifetimes3,5.

What is needed to map conformational rearrangements in proteins is a technique that can work over shorter distances than classical FRET. We have developed such a method called “transition metal ion FRET”, which has shorter R_0 values (about 10 Å), uses small dyes with short linkers, and is not sensitive to the orientation problems usually associated with FRET. Unlike NMR, EPR, and crystallography, transition metal ion FRET could theoretically be applied to proteins of any size, in membranes, on extracellular domains of proteins in living cells, and potentially on single molecules. It can measure the kinetics of the conformational change in real time and can be paired with other functional measurements. Here, we utilize this method along with x-ray crystallography to explore the conformational motions of the carboxyl terminal region of HCN2 during ligand-activation. Our results demonstrate the ability of transition metal ion FRET to reveal structural rearrangements in proteins and provide a model for allosteric movements of HCN2.

RESULTS

Transition metal ion FRET

Our fluorescence method relies on two previous observations. First, transition metal ions such as Ni^{2+} and Cu^{2+} are colored and their weak absorbances overlap with the emission of fluorescent dyes including fluorescein (Fig. 1a). Thus, Ni^{2+} and Cu^{2+} can be used as short-range FRET acceptors6,7. Indeed, the R_0 for Ni^{2+} and fluorescein (12 Å) is 4 times shorter than standard FRET pairs such as CFP, YFP (50 Å) or fluorescein, rhodamine (54 Å) 8,9. The R_0 value between Cu^{2+} and fluorescein is longer (16 Å), allowing transition metal ion FRET to be tuned to different distance ranges. Second, a metal-binding site can be engineered into proteins with minimal perturbation to the backbone by introducing two histidines spaced one turn away on an α-helix (Fig. 1b) 10,11. We reasoned that by engineering a metal ion-binding motif into α-helices, and by introducing a fluorophore such as fluorescein onto a cysteine residue, we could use FRET to observe small conformational

rearrangements in proteins. The efficiency of FRET (*E*), and hence the distance between the donor and acceptor, can easily be determined by measuring fluorescence before *(F)* and after *(F_{metal})* the addition of metals ($E = 1\text{-}F_{metal}/F$). To test the use of transition metal ions as short-range FRET acceptors, we measured FRET in a set of model α-helical peptides based on the sequence AAAAKAAAKAAAAAKA. The peptides contained a single reactive cysteine at the second amino acid position (C2) and a pair of histidines spaced at increasing distances along one face of the helix (Fig. 1b). We modified the cysteine with the reactive fluorophore fluorescein-5-maleimide (F5M). We performed fluorescence quenching experiments on the peptides in solution. In a peptide with a metal binding site adjacent to the fluorophore (C2H3H6), we observed substantial quenching of the emission spectrum of fluorescein with increasing concentrations of Ni^{2+} (Fig. 1c). While 1 mM Ni^{2+} produced no appreciable FRET $(1\text{-}F_{metal}/F)$ in the $C2_{F5M}$ control peptide containing no histidines (3% ± 4 %), FRET efficiency decreased with distance in peptides containing the di-histidine motif: C2H3H6 (43% ± 4 %); C2H6H10 (27% ± 4%); and C2H10H14 (13% ± 2%) (Fig. 1d). The small decrease in fluorescence seen in the $C2_{F5M}$ control at 10 mM Ni^{2+} was likely due to collisional quenching of fluorescein by Ni^{2+} in solution and had a Stern-Volmer quenching constant (K_{sv}) of 18 M^{-1} (Supplementary Fig. 1). These data indicate that Ni^{2+} can be used as a close-range distance-dependent acceptor for fluorescein. Cu^{2+}, which has a longer R_0 than Ni^{2+}, exhibited more robust distance-dependent FRET with fluorescein-modifed peptides: C2H3H6 (84% ± 5); C2H6H10 (77% ± 2); and C2H10H14 (50% ± 7%) (Fig. 1e).

To demonstrate that our data could be explained by a FRET mechanism, we compared distances calculated from FRET to distances predicted from model peptides (Fig. 1f). Assuming an α-helical structure of the peptide and a modeled position of the fluorophore and metal binding site, the FRET efficiencies obtained for both Ni^{2+} and Cu^{2+} at all three metal ion binding-sites are fit well by the Forster equation with R_0 values of 12 Å and 16 Å for Ni^{2+} and Cu^{2+} respectively. These results support the idea that quenching occurred by a FRET mechanism.

FRET measurements of the HCN2 holo state

Cyclic nucleotide-binding domains (CNBD) are found in a variety of proteins. The domain consists of a β-roll and a carboxyl-terminal α-helical region (B- and C-helix), which caps the cAMP-binding site (Fig. 2a). In each of the subunits of the cyclic nucleotide-regulated ion channel HCN2, a CNBD is linked through a series of 6 helices (C-linker) to a transmembrane pore-forming region12. HCN2 channel subunits assemble as a symmetric tetramer to form an ion-conducting pore and a cytosolic gating ring made from the C-linker and CNBD from each subunit (Fig. 2b). In cyclic nucleotide-regulated channels, the binding of cAMP to the CNBD stabilizes conformational rearrangements that propagate up through the C-linker and allow the pore to open12.

Previous models of how cAMP activates HCN2 channels have suggested that structural changes in the C-helix and C-linker occur12. To elucidate the structural transitions that occur in these regions, we mutated, expressed, and purified a cysteine-less version of the carboxyl-terminal region of HCN2. While a tetramer in the channel, this fragment is a monomer in solution1. We solved the X-ray crystal structure of this fragment bound to

cAMP (holo state). The structure was virtually identical to that of the wild-type holo state HCN2 (RMSD of main chain atoms is 0.7 Å) (Fig. 2a,b and Supplementary Table 1)1. We then introduced single cysteines at surface-exposed sites in the F′-helix of the C-linker (N520C) or in the β-roll of the CNBD (K570C) and covalently modified them with fluorescein-5-maleimide. We introduced Ni^{2+}-binding motifs (His-X_3-His) at 4 positions along the C-helix: M620H, A624H; A624H, V628H; T627H, D631H; and I630H, D634H. To map distances in the holo state, we measured the fluorescence with increasing concentrations of Ni^{2+} (Fig. 2c). All measurements were done at saturating concentration of cAMP (250 μM) (Supplementary Fig. 2). Constructs labeled at N520C in the C-linker showed robust concentration-dependent FRET that plateaued at about 500 μM Ni^{2+} (Fig. 2c). Notably, at 500 μM Ni^{2+}, each metal-binding site exhibited a different amount of FRET: M620H, A624H (66.9% ± 1.7%); A624H, V628H (77.3% ± 2.7%); T627H, D631H (74.9% ± 1.2%); and I630H, D634H (43.5% ± 2.3%) (Fig. 2c). Constructs labeled at K570C in the β-roll also produced significant FRET values at saturating Ni^{2+}: M620H, A624H (30.3% ± 1.9%); A624H, V628H (29.4% ± 1.7%); T627H, D631H (37.4% ± 1.6%); and I630H, D634H (36.2% ± 1.8%) (Fig. 2d).

Unexpectedly, the control channel construct $N520C_{F5M}$ which contains no engineered Ni^{2+}-binding motifs also showed Ni^{2+}-dependent FRET (27.2% ± 3.5%) (Fig. 2c). Cu^{2+} produced a larger amount of FRET in the control $N520C_{F5M}$ (Supplementary Fig. 3)6,7. The large Cu^{2+}-dependent FRET signal in the control barred the use of Cu^{2+} to map distances in HCN2. However, these data are consistent with the background quenching being the result of FRET between a native metal-ion binding site in HCN2 and $N520C_{F5M}$. While the Ni^{2+} effect was smaller and somewhat lower affinity (44 μM) than that of the constructs with engineered Ni^{2+}-binding motifs, it was still higher affinity than that of the control peptide containing no histidines ($C2_{F5M}$) (>50 mM) (Fig. 1c and Supplementary Fig. 1). These results suggest that the HCN2 carboxyl-terminal region contains a native metal ion-binding site near the F′-helix. In the $K570C_{F5M}$ control channel fragment, the native Ni^{2+}-binding site produced less FRET (18.2% ± 2.6%), indicating that the native Ni^{2+} site is farther from $K570C_{F5M}$ than $N520C_{F5M}$ (Fig. 2d).

To relate the holo state structure of the HCN2 carboxyl-terminal fragment in solution to the crystal structure, we compared distances determined from FRET to distances determined from X-ray crystallography. We calculated distances from FRET efficiencies using a Forster equation that took into account FRET from the native Ni^{2+} binding sites and assumed random orientation of the donor and acceptor. This is a reasonable assumption given the anisotropy of the fluorophores ($N520C_{F5M}$ 0.216±0.001, $K570C_{F5M}$ 0.178±0.002) (Supplementary Fig. 4) and the multiple absorption dipoles of the Ni^{2+} ions13,14. To separate the specific FRET signal of the engineered di-histidine sites from the native Ni^{2+} binding site we used a version of the Forster equation that considers FRET to multiple acceptors and held the distance to the native site constant15–18. While we do not know if there is one or multiple native metal sites, a single apparent distance term could be used to correct FRET signals15–18. Using spatial coordinates from the holo HCN2 crystal structure, we modeled the Ni^{2+}-binding motifs into constrained positions along the C-helix. Fluorophore positions (modeled as a point source) that fit the experimental FRET distances were found using a best-fit least-squares analysis. Figure 2e and Supplementary Figure 5

shows one possible position of the dye that overlapped the point source. The modeled distances closely match our experimental values (Fig. 2f) with a RMSD of 2 Å. The single outlier likely resulted from difficulties in measuring distances far from R_0 Movements of excited state fluorophores or a distribution of fluorophore positions can bias FRET measurements towards shorter distances or R_0 respectively9. From this analysis combined with our measurements on peptides (Fig. 1) we conclude that the structure in solution closely matches the structure in the crystal, and that our FRET method can map spatial positions within proteins.

X-ray crystal structure of the HCN2 apo state

To understand how cAMP-binding changes the conformation of HCN2, we solved the x-ray crystal structure of the wild-type HCN2 carboxyl-terminal fragment in the absence of cAMP (apo state) (Fig. 3a,b and Supplementary Table 1). Surprisingly, the overall structure is very similar to that of the holo state (Fig. 3c). The first 5 helices of the C-linker as well as the β-roll are virtually identical (RMSD 0.5 Å). We could resolve several bromide ions in the structure with two located in the cyclic nucleotide binding pocket, one of which occupies the position equivalent to the phosphate group of cAMP in the holo state structure (Supplementary Fig. 6). We observed two major differences between the holo and apo state structures. First, the F′-helix adopts a less helical structure in the apo state (Fig. 3c,d). Second, the carboxyl-terminal portion of the C-helix was no longer resolved, indicating that the end of the C-helix becomes less ordered. This lack of structural information of the carboxyl-terminal portion of the C-helix precludes us from determining the precise conformation of the C-helix in the apo state via crystallography. Furthermore, the small α-helical amino-terminal portion of the C-helix visible in the apo-state crystal, which was nearly identical to the holo state structure, was involved in crystal contacts between tetramers and therefore might not accurately represent the solution structure of this region (Supplementary Fig. 7). Nevertheless, these data suggest that cAMP-dependent rearrangements occur in the F′- and C-helices.

FRET measurements of cAMP-induced structural changes

Because we were unable to fully determine the rearrangements of the C-helix from crystallography, we turned to our transition metal ion FRET method. The Ni^{2+}-dependence of FRET was measured for each of the previous constructs, this time without cAMP (Fig. 4a,b). The control construct containing $N520C_{F5M}$ in the F′-helix and no engineered Ni^{2+}-binding motifs exhibited a small decrease in FRET in the absence of cAMP, consistent with a small change in distance between this position and the native Ni^{2+}-binding site (Fig. 4c). We did not observe this change with $K570C_{F5M}$, which indicates that, while the native Ni^{2+} site is stationary, the F′-helix ($N520C_{F5M}$) makes a small movement during cAMP binding. These data are consistent with both the crystallography data and previous studies of CNGA1 channels19. We observed changes in FRET for all of the $N520C_{F5M}$ and $K570C_{F5M}$ constructs containing engineered Ni^{2+}-binding sites in the C-helix (Fig. 4c). To translate FRET changes into distances, we calculated distance changes (holo vs. apo) according to the Forster equation taking into account FRET from the native Ni^{2+}-binding site15–18. We detected large movements between both $N520C_{F5M}$ and $K570C_{F5M}$ and the first and second pair of histidines in the C-helix (Fig. 4c). In contrast, the middle and end of the C-helix

(T627H, D631H and I630H, D634H) showed only small changes in distance. Since these movements were also detected with the fluorophore at K570C, which undergoes little or no movement itself, it seems highly likely that the FRET changes we observed arise primarily from movements of the C-helix and not movements of the fluorophores themselves. At every position, FRET increased upon cAMP-binding, which suggests that the C-helix, particularly the amino-terminal end of the C-helix, translates toward the β-roll of the CNBD.

Along with distance measurements, our FRET method provides information about protein secondary structure. The affinity of di-histidine motifs for transition metal ions is sensitive to helix stability10,11,20. Indeed, while individual metal binding sites within the same proteins can have diverse Kd's, helix stability tends to increases the affinity of engineered sites for metal11,20,21. In HCN2, cAMP-binding caused a significant increase in the affinity for Ni^{2+} at each introduced Ni^{2+}-binding site (but not the native sites) in $N520C_{F5M}$ ($P < 0.05$, student's t-test) (Fig. 5a and Supplementary Table 2). We observed a similar increase in affinity for proteins labeled at $K570C_{F5M}$ (Fig. 5b and Supplementary Table 2). The large shifts in Ni^{2+} affinity correspond to Δ Δ G values between − 0.4 and − 1.7 kcal/mol, values similar to the energetics of helix stabilization observed in other systems11,20,21. The observed shifts indicate that cAMP-binding stabilizes the α-helical structure of the C-helix. These data demonstrate the ability of metal ion FRET to reveal secondary structure transitions in proteins.

DISCUSSION

Until now, models of CNBD dynamics suggested that the C-helix makes a rigid-body movement to cap the CNBD12,22. Crystal structures of CNBD-containing proteins including protein kinase A (PKA), exchange protein activated by cAMP (EPAC), and the bacterial cyclic nucleotide regulated channel *M. loti* K have shown movements of the C-helix in response to cAMP-binding23–25. Each of these structures shows different and sometimes large conformational rearrangements. In the *M. Loti* K channel alone, x-ray crystallography revealed six distinct conformations of the C-helix, making it difficult to infer how the C-helix actually moves in solution23. Clearly, it is sometimes difficult to determine the conformational motions of a protein from crystal structures alone.

For HCN2, crystallography did not reveal substantial differences in the resolved portion of the C-helix between the holo and apo states. We believe that crystal contacts in this region likely stabilized the C-helix in a non-physiological conformation. With transition metal ion FRET, however, we measured cAMP-induced rearrangements of the C-helix in solution, an environment that more accurately represents the physiological state of the protein. Our results suggest that, coupled to ligand-binding, the amino-terminal end of the C-helix moves towards the core of the CNBD, swinging several angstroms towards the β-roll (Fig. 5c). Also, the entire C-helix and F′-helix adopt a more α-helical secondary structure (Fig. 5c). Since the amino-terminal end of the C-helix is very near the F′-helix, these results suggest a mechanism where the movement of the C-helix in the CNBD is coupled to a movement of the F′-helix in the C-linker. These rearrangements could likely be the start of the conformational wave that propagates up through the C-linker to stabilize the open conformation of the channel pore.

Transition metal ion FRET has seven key features that are likely to make it useful for studying the intramolecular movements of proteins. (1) The short R_0 allows close-range distances to be monitored. (2) It is compatible with small, bright fluorophores and metal ions, with little or no linker which should better represent the structure and conformational changes of the protein backbone. (3) The multiple transition dipoles of the metal ion acceptor greatly reduce the orientation dependence of FRET14,26. (4) The donor and acceptor can be introduced independently at two different sites. (5) The metal ion acceptor can be added and removed to measure absolute FRET efficiency by donor quenching/de-quenching measurements. (6) Transitions in secondary structure can be monitored by measuring the affinity of the metal-binding site. (7) Lastly, different colored transition metal ions can be used to measure distances in different dynamic ranges6,7,26. Future extension of the method to single molecule measurements should allow the stochastic movements of individual proteins to be measured. These measurements could in principal help determine the structures of rare conformational states which would be hidden in population measurements. We anticipate that this technique will be useful in future studies of the nature of protein conformational changes.

METHODS

Protein preparation for crystallography of wild-type HCN2I apo state and cysteine-less HCN2I holo state

For preparation of the cysteine-less HCN2I fragment, a DNA fragment encoding residues 443–640 of the mouse HCN2 ion channel was synthesized (Blue Heron Biotechnology) and cloned into the pMAL-c2T expression vector (New England Biolabs). The three native cysteines were mutated as follows: C508N, C584S, C601S. Protein was prepared as previously described27. The wild-type mouse HCN2I construct (residues 443–640) was prepared as previously described, but after ion exchange purification, the protein was dialyzed in buffers without cAMP1.

Crystallography

Crystals were grown by the hanging drop, vapor diffusion method at 4° C. Co-crystals of HCN2I-cysless and cAMP grew using a 1:1 mixture of protein and reservoir solution composed of 16% w/v PEG 6000, 500 mM NaCl, 10% glycerol, and 100 mM citrate (pH 5). These conditions produced tetragonal crystals within 3 days with space group P4212 that diffracted to a resolution of 1.9 Å. HCN2I-apo crystals grew using a 2:1 mixture of protein and reservoir solution composed of 20% w/v PEG 8000, 400 mM NaCl, 100 mM NaBr, 20% glycerol, and 100 mM MES (pH 6.0). Crystals grew within 8 weeks and were harvested an additional eight weeks after initial growth.

For diffraction data collection, crystals were immersed in liquid nitrogen without further cryoprotectant-soaking. For HCN2I-cysfree cAMP co-crystals, diffraction data were collected at 110 K on beamline 8.2.1 at ALS. For HCN2I apo crystals, data were collected at beamline X26C of NSLS with x-rays tuned to the bromine edge calculated by a fluorescence scan of the crystal. Integration, scaling and merging of the diffraction data were done with the HKL suite of programs (http://www.hkl-xray.com). The structures were solved by

molecular replacement using the programs Phaser, MOLREP, and AmoRe28,29. For cAMP-bound HCN2I-cysfree, the structure of HCN2J+cAMP (1Q5O) was used as a search probe. For apo HCN2I the structure of HCN2I+cAMP (1Q43) without the ligand or C-helix was used as a search probe. Model rebuilding was accomplished with the program O30, and COOT31 using F_o-F_c "omit" maps and refinement was carried out using REFMAC-5 32 and ARP/wARP32. Parameters used to define the stereochemistry of cAMP were derived from the corresponding small-molecule crystal structures obtained from the Cambridge Structure Database (http://www.ccdc.cam.ac.uk). Five percent of the data were used to calculate the R_{free} for cross-validation of the refinement process33. Additional crystallographic calculations and graphics employed the program suites of CNS34,35 and Uppsala Software Factory. The data processing and refinement statistics are given in Supplementary Table 1. The atomic coordinates for each structure have been deposited in the Protein Data Bank (3ETQ, 3FFQ).

Protein preparation for fluorescence

Cysteines and histidines were introduced into the cysteine-less HCN2I sequence with PCR mutagenesis as previously described19. All constructs were confirmed by DNA sequencing. Protein was prepared as described above with the following modifications: protein was eluted into maltose buffer without TCEP and labeled with 100 μM fluorescein-5-maleimide (Invitrogen) for 3 h at room temperature. After thrombin cleavage, fluorescein-labeled protein was diluted, loaded on an ion exchange column (GE Healthcare), and eluted as a single fluorescent peak with a linear KCl gradient.

Peptides

Peptides (ACAAKAAAKAAAAAKA, ACHAKHAAKAAAAAKA, ACAAKHAAKHAAAAKA, ACAAKAAAKHAAAHKA) were synthesized with N-terminal acetylation and C-terminal amidation (American Peptide Company) and diluted to a concentration of 20 μM in MOPS buffer (260 NaCl, 60 MOPS, pH 7.2). Peptides were labeled with 100 μM fluorescein-5-maleimide for 2 h at room temperature. Labeled peptides were purified as a single peak from unincorporated dye by fluorescence size exclusion chromatography (Shimadzu) using a Superdex Peptide 10/300 column (GE Healthcare).

Fluorometry and spectroscopy

Fluorescently-labeled protein was diluted to a concentration of 20–80 nM in 2X fluorescence buffer (260 mM NaCl, 6 mM HEPES, pH 7.2). For Ni^{2+}-binding curves, protein was mixed with an equal volume of Ni^{2+} solution in water and kept on ice. For holo state experiments, 250 μM cAMP was added to the solution. Steady-state fluorescence emission spectra were acquired with a Fluorolog-3 fluorometer (Horiba Jobin Yvon). Ni^{2+}-binding curves of model peptides were measured as above with the following modification: FPLC purified peptide was mixed with Ni^{2+} in MOPS buffer along with 2,2,2-trifluoroethanol (final concentration 50% v/v) (Sigma). The absorbance of Ni^{2+} and Cu^{2+} bound to an unlabeled di-histidine model peptide (ACAAKAAAKHAAAHKA) was determined at 3:1 peptide/metal ratio using a Beckman DU 640 spectrophotometer.

Fluorescence data analysis of peptides

Fluorescence values were averaged over an 11 nm window surrounding the peak of the spectrum. All spectra were blank corrected and normalized to the fluorescence before the addition of metals. Fluorescence was corrected for the inner filter effect of metals9. Data for the control C2 peptides were fitted to a single-site binding curve model with the following equation:

$$\frac{F_{metal}}{F} = \frac{1}{1+\frac{[metal]}{Kd_1}}$$

F_{metal} is the fluorescence of the donor in the presence of metal, F is the fluorescence of the donor without metal, and Kd_1 is the equilibrium dissociation constant for collisional quenching. Data for peptides containing engineered metal binding sites were fitted with a two-site binding curve model with the following equation to account for non-specific solution quenching of the fluorophore:

$$\frac{F_{metal}}{F} = \left(1 - \frac{E}{1+\frac{Kd_2}{[metal]}}\right)\left(\frac{1}{1+\frac{[metal]}{Kd_1}}\right)$$

E is the FRET efficiency, and Kd_2 is the equilibrium dissociation constant for the engineered metal binding sites. The distances between the fluorophore and the metal were calculated using the Forster equation: $R = R_0\,(1/E\text{-}1)^{1/6}$. R is the distance between the fluorophore and the metal and R_0 is the Forster distance. R_0 was calculated as previous described2,19. Quenching of fluorescein-labeled peptide by high concentrations of Ni^{2+} in solution was quantified by fitting a Stern-Volmer equation where K_{SV} is the Stern-Volmer quenching constant:

$$\frac{F}{F - F_{metal}} = 1 + \frac{1}{K_{sv}[Ni^{2+}]}$$

Fluorescence data analysis of proteins

FRET data from protein constructs were fitted to a single-site binding curve model with the following equation:

$$\frac{F_{metal}}{F} = 1 - \frac{E}{1+\frac{Kd}{[Ni^{2+}]}}$$

F_{metal} is the fluorescence of the donor in the presence of Ni^{2+}, F is the fluorescence of the donor without Ni^{2+}, E is the FRET efficiency, and Kd is the equilibrium dissociation constant for Ni^{2+}. Fitting the data with a two-site binding model did not produce significantly better fits. The distance (R_B) between each fluorophore and the native Ni^{2+}-binding site in the HCN2I protein were calculated using the Forster equation. For constructs

containing di-histidine Ni^{2+} motifs in the C-helix, our measured FRET values (E_{total}) were the combination of FRET to the native Ni^{2+} binding site (distance of R_B) as well as the engineered sites (distance of R). Thus, the following equation for FRET between one donor and multiple acceptors can be used15–18:

$$E_{total}=\frac{R_0^6\left(\frac{1}{R^6}+\frac{1}{R_B^6}\right)}{1+R_0^6\left(\frac{1}{R^6}+\frac{1}{R_B^6}\right)}$$

This equation can be rearranged to calculate the distance (R) to each engineered Ni^{2+}-binding motif, correcting for the native site:

$$R=\sqrt[6]{\frac{1-E_{total}}{\frac{E_{total}}{R_0^6}+\frac{1}{R_B^6}(E_{total}-1)}}$$

While we do not yet know whether the native FRET we observe was due to one or multiple Ni^{2+} ions bound to the protein, for the purposes of this correction, FRET from multiple native Ni^{2+} ions is mathematically equivalent to FRET from a single native Ni^{2+} ion with distance (R_B) 15–18. Anisotropy was measured with a Fluorolog-3 fluorometer (Horiba Jobin Yvon) and calculated using the anisotropy package in FluorEssence Software (Horiba Jobin Yvon). All error bars are ± s.e.m.

Structural modeling

The position of the metal ion at each site was estimated from models of α-helical peptides built using PYMOL and a survey of crystal structures of metal-binding proteins from the Protein Data Bank36–39. To model positions of the fluorophore, distances between each metal-binding motif and the fluorophore were calculated from FRET. Distances were then calculated for both Cu^{2+} and Ni^{2+} at each metal binding site and a test position of the fluorophore. Using the solver function of Excel (Microsoft), a position of the fluorophore was found that yielded the best fit (by a least-squares method) between the predicted and experimental distances to all three metal-binding sites19. To model positions of the fluorophores in HCN2 the location of the Ni^{2+} ion at each site was estimated from the HCN2 crystal structure1. Distances were calculated between each Ni^{2+} position and a test position of the fluorophore as described above.

Supplementary Material

Refer to Web version on PubMed Central for supplementary material.

Acknowledgments

We are grateful to K. Black, S. Cunnington, S. Simmons, and G. Sheridan for technical assistance. We thank the beamline staff at ALS and NSLS. We thank W. Almers, B. Hille, and A. Merz for comments on the manuscript. We thank E. Gouaux and L. Islas for stimulating discussions. This work was supported by the Howard Hughes Medical Institute and National Institutesof Health Grants (EY10329) to W. Zagotta and (R01 NS038631) to E. Gouaux.

M.C.P was supported by an NRSA fellowship from the National Eye Institute. J.W.T was supported by a fellowship from the Jane Coffin Childs Foundation and a NIH Pathway to Independence Award (1K99NS064213).

References

1. Zagotta WN, et al. Structural basis for modulation and agonist specificity of HCN pacemaker channels. Nature. 2003; 425:200–5. [PubMed: 12968185]
2. Selvin PR. Fluorescence resonance energy transfer. Methods Enzymol. 1995; 246:300–34. [PubMed: 7752929]
3. Posson DJ, Selvin PR. Extent of voltage sensor movement during gating of shaker K+ channels. Neuron. 2008; 59:98–109. [PubMed: 18614032]
4. Best RB, et al. Effect of flexibility and cis residues in single-molecule FRET studies of polyproline. Proc Natl Acad Sci U S A. 2007; 104:18964–9. [PubMed: 18029448]
5. Selvin PR. Principles and biophysical applications of lanthanide-based probes. Annu Rev Biophys Biomol Struct. 2002; 31:275–302. [PubMed: 11988471]
6. Richmond TA, Takahashi TT, Shimkhada R, Bernsdorf J. Engineered metal binding sites on green fluorescence protein. Biochem Biophys Res Commun. 2000; 268:462–5. [PubMed: 10679227]
7. Sandtner W, Bezanilla F, Correa AM. In vivo measurement of intramolecular distances using genetically encoded reporters. Biophys J. 2007; 93:L45–7. [PubMed: 17766346]
8. Vogel SS, Thaler C, Koushik SV. Fanciful FRET. Sci STKE. 2006:re2. [PubMed: 16622184]
9. Lakowicz, JR. Principles of fluorescence spectroscopy. Vol. xxiii. Kluwer Academic/Plenum; New York: 1999. p. 698
10. Arnold FH, Haymore BL. Engineered metal-binding proteins: purification to protein folding. Science. 1991; 252:1796–7. [PubMed: 1648261]
11. Suh SS, Haymore BL, Arnold FH. Characterization of His-X3-His sites in alpha-helices of synthetic metal-binding bovine somatotropin. Protein Eng. 1991; 4:301–5. [PubMed: 1713327]
12. Craven KB, Zagotta WN. CNG and HCN channels: two peas, one pod. Annu Rev Physiol. 2006; 68:375–401. [PubMed: 16460277]
13. Dale RE, Eisinger J, Blumberg WE. The orientational freedom of molecular probes. The orientation factor in intramolecular energy transfer. Biophys J. 1979; 26:161–93. [PubMed: 262414]
14. Figgis, BN.; Hitchman, MA. Ligand field theory and its applications. Vol. xviii. Wiley-VCH; New York: 2000. p. 354
15. Forster T. Experimentelle Und Theoretische Untersuchung Des Zwischenmolekularen Ubergangs Von Elektronenanregungsenergie. Zeitschrift Fur Naturforschung Section a-a Journal of Physical Sciences. 1949; 4:321–327.
16. Wolber PK, Hudson BS. An analytic solution to the Forster energy transfer problem in two dimensions. Biophys J. 1979; 28:197–210. [PubMed: 262548]
17. Zimet DB, Thevenin BJ, Verkman AS, Shohet SB, Abney JR. Calculation of resonance energy transfer in crowded biological membranes. Biophys J. 1995; 68:1592–603. [PubMed: 7787045]
18. Miranda P, et al. FRET with multiply labeled HERG K(+) channels as a reporter of the in vivo coarse architecture of the cytoplasmic domains. Biochim Biophys Acta. 2008; 1783:1681–99. [PubMed: 18634834]
19. Taraska JW, Zagotta WN. Structural dynamics in the gating ring of cyclic nucleotide-gated ion channels. Nat Struct Mol Biol. 2007; 14:854–60. [PubMed: 17694071]
20. Kellis JT Jr, Todd RJ, Arnold FH. Protein stabilization by engineered metal chelation. Biotechnology (N Y). 1991; 9:994–5. [PubMed: 1369354]
21. Todd RJ, Van Dam ME, Casimiro D, Haymore BL, Arnold FH. Cu(II)-binding properties of a cytochrome c with a synthetic metal-binding site: His-X3-His in an alpha-helix. Proteins. 1991; 10:156–61. [PubMed: 1654548]
22. Rehmann H, Wittinghofer A, Bos JL. Capturing cyclic nucleotides in action: snapshots from crystallographic studies. Nat Rev Mol Cell Biol. 2007; 8:63–73. [PubMed: 17183361]

23. Altieri SL, et al. Structural and energetic analysis of activation by a cyclic nucleotide binding domain. J Mol Biol. 2008; 381:655–69. [PubMed: 18619611]
24. Kim C, Xuong NH, Taylor SS. Crystal structure of a complex between the catalytic and regulatory (RIalpha) subunits of PKA. Science. 2005; 307:690–6. [PubMed: 15692043]
25. Rehmann H, Das J, Knipscheer P, Wittinghofer A, Bos JL. Structure of the cyclic-AMP-responsive exchange factor Epac2 in its auto-inhibited state. Nature. 2006; 439:625–8. [PubMed: 16452984]
26. Horrocks WD Jr, Holmquist B, Vallee BL. Energy transfer between terbium (III) and cobalt (II) in thermolysin: a new class of metal--metal distance probes. Proc Natl Acad Sci U S A. 1975; 72:4764–8. [PubMed: 1061067]
27. Flynn GE, Black KD, Islas LD, Sankaran B, Zagotta WN. Structure and rearrangements in the carboxy-terminal region of SpIH channels. Structure. 2007; 15:671–82. [PubMed: 17562314]
28. McCoy AJ. Solving structures of protein complexes by molecular replacement with Phaser. Acta Crystallogr D Biol Crystallogr. 2007; 63:32–41. [PubMed: 17164524]
29. Navaza J. Amore - an Automated Package for Molecular Replacement. Acta Crystallographica Section A. 1994; 50:157–163.
30. Jones TA, Zou JY, Cowan SW, Kjeldgaard M. Improved Methods for Building Protein Models in Electron-Density Maps and the Location of Errors in These Models. Acta Crystallographica Section A. 1991; 47:110–119.
31. Emsley P, Cowtan K. Coot: model-building tools for molecular graphics. Acta Crystallogr D Biol Crystallogr. 2004; 60:2126–32. [PubMed: 15572765]
32. Murshudov GN, Vagin AA, Dodson EJ. Refinement of macromolecular structures by the maximum-likelihood method. Acta Crystallogr D Biol Crystallogr. 1997; 53:240–55. [PubMed: 15299926]
33. Brunger AT. Assessment of Phase Accuracy by Cross Validation - the Free R-Value -Methods and Applications. Acta Crystallographica Section D-Biological Crystallography. 1993; 49:24–36.
34. The CCP4 suite: programs for protein crystallography. Acta Crystallogr D Biol Crystallogr. 1994; 50:760–3. [PubMed: 15299374]
35. Brunger AT, et al. Crystallography & NMR system: A new software suite for macromolecular structure determination. Acta Crystallographica Section D-Biological Crystallography. 1998; 54:905–921.
36. DeLano, WL. The PyMOL Molecular Graphics System. DeLano Scientific LLC; Palo Alto, CA, USA: 2008.
37. Schreiter ER, et al. Crystal structure of the nickel-responsive transcription factor NikR. Nat Struct Biol. 2003; 10:794–9. [PubMed: 12970756]
38. Telmer PG, Shilton BH. Structural studies of an engineered zinc biosensor reveal an unanticipated mode of zinc binding. J Mol Biol. 2005; 354:829–40. [PubMed: 16288781]
39. Wray JW, Baase WA, Ostheimer GJ, Zhang XJ, Matthews BW. Use of a non-rigid region in T4 lysozyme to design an adaptable metal-binding site. Protein Eng. 2000; 13:313–21. [PubMed: 10835104]

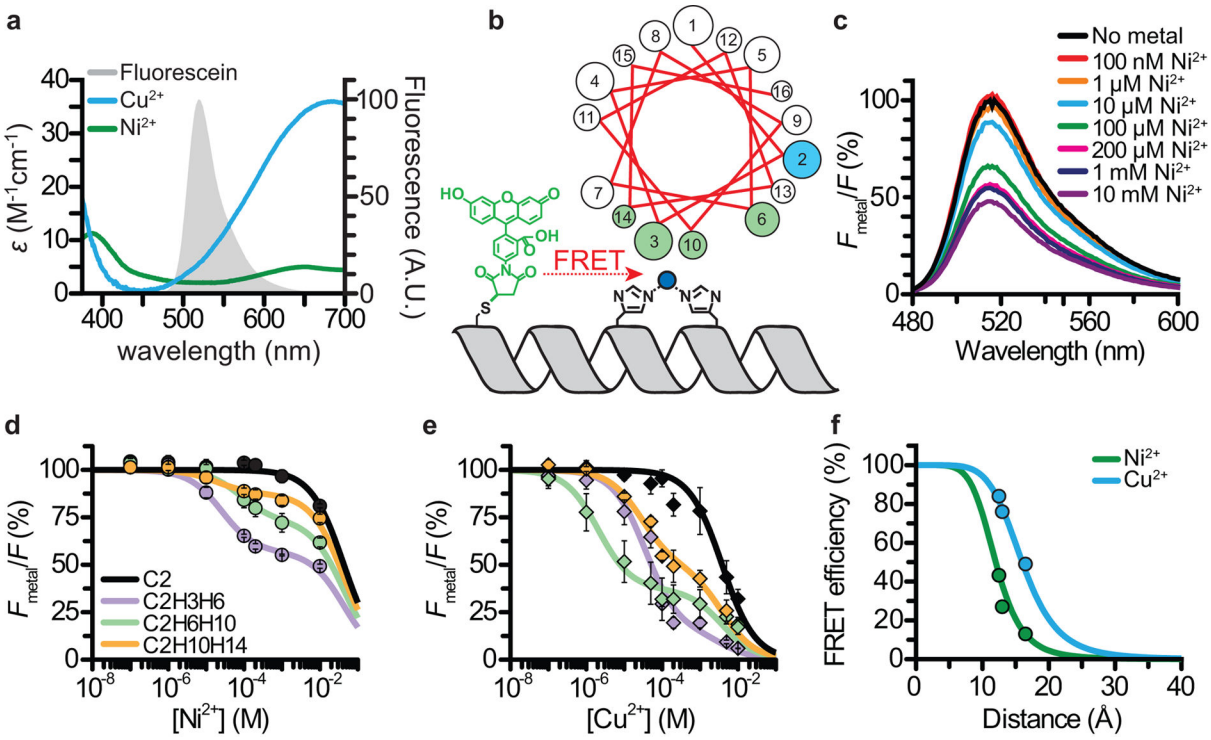

Figure 1.

Measuring distances with transition metal ion FRET. (**a**) Spectral overlap between fluorescein emission (grey) and the absorbance of Ni^{2+} (green line) and Cu^{2+} (blue line) bound to the peptide ACAAKAAAKHAAAHKA. (**b**) Cartoon of FRET between a fluorescein-modified cysteine and a Ni^{2+}-binding motif in an α-helix. A helical wheel projection of the position of the cysteine (blue) and histidine (green) residues in the model peptides. (**c**) Quenching of fluorescein by increasing concentrations of Ni^{2+} in the model peptide AC_{F5M}HAKHAAKAAAAAKA. (**d**) Average quenching of model peptides AC_{F5M}AAKAAAKAAAAAKA (black), AC_{F5M}HAKHAAKAAAAAKA (purple), AC_{F5M}AAKHAAKHAAAAKA (green), and AC_{F5M}AAKAAAKHAAAHKA (orange). Fluorescence was normalized to the intensity before the addition of Ni^{2+}. Data were fit to a single-site binding model (solid line). (**e**) Average quenching of fluorescein by Cu^{2+} in the same peptides as **c**. Error bars are s.e.m. (n = 4–6). (**f**) Comparison of modeled distances to experimental FRET values in all peptides with Ni^{2+} and Cu^{2+}.

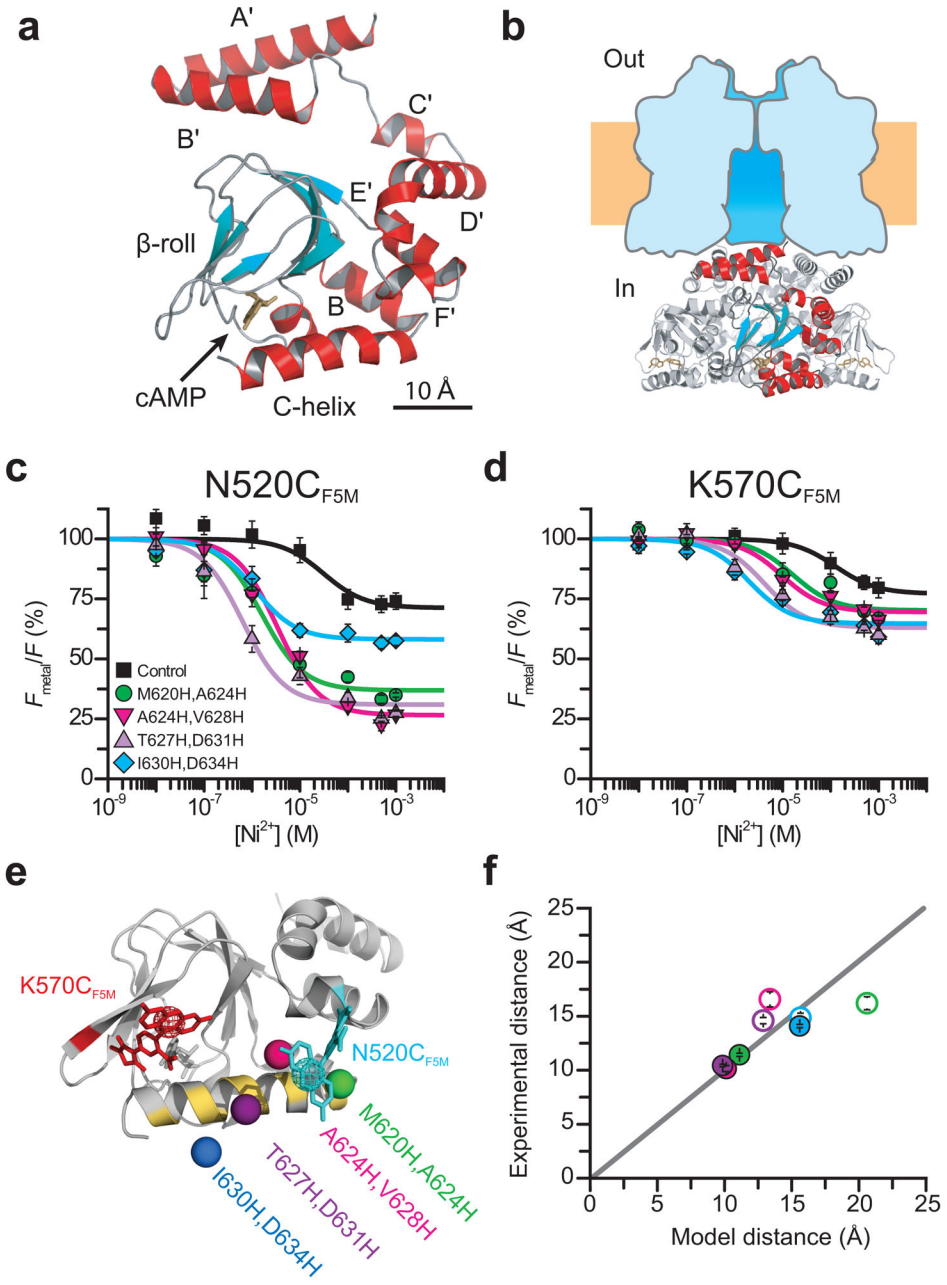

Figure 2.

Mapping distances in HCN2 bound to cAMP with transition metal ion FRET. (**a**) X-ray crystal structure of a single subunit of the cysteineless HCN2 carboxyl-terminal fragment (Clinker and CNBD) bound to cAMP. (**b**) Organization of the tetrameric complex viewed parallel to the membrane. Cartoon of transmembrane domain based on the structure of Kv1.2 is shown in blue. (**c,d**) Plots of Ni^{2+}-dependent quenching of HCN2 constructs labeled with fluorescein-5-maleimide at N520C (**c**) or K570C (**d**) with Ni^{2+}-binding motifs in the C-helix. Control contains no introduced histidines. Fluorescence was measured in solution containing 250 μM cAMP, normalized to the intensity before the addition of Ni^{2+},

and fit by a single-site binding model (solid lines). Error bars are s.e.m. (n = 4–6). (**e**) Structural model for positions of fluorescein-5-maleimide conjugated to N520C (cyan) and K570C (red) in relation to the 4 Ni^{2+}-binding motifs. Point sources used for calculations are shown as mesh spheres. (**f**) Plot of distances determined from FRET (experimental) for each position compared to distances determined from the crystal structure (model). Error bars are s.e.m. (n = 4–6). Colors match **c** with open circles corresponding to distances to $K570C_{F5M}$ and closed circles distances to $N520C_{F5M}$.

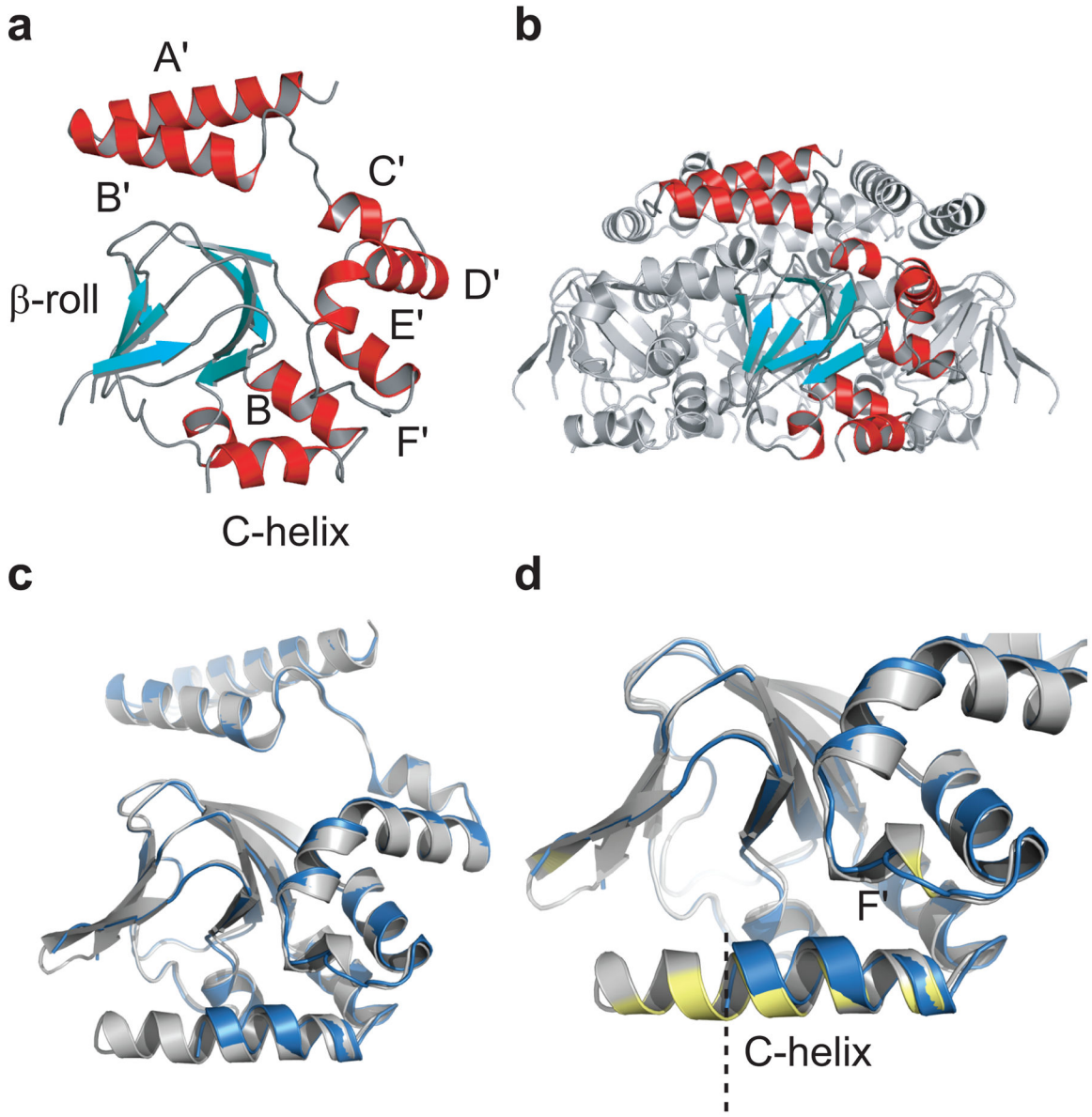

Figure 3.

Crystal structure of the mouse wild-type HCN2 carboxyl-terminal fragment (C-linker and CNBD) in the absence of cAMP. Ribbon diagram of a single subunit (**a**) and tetrameric organization (**b**) of the apo state. (**c**) Overlay of the apo (blue) and holo (grey) state HCN2 crystal structures. (**d**) Expanded view of the structural differences in the F′- and C-helices that occur as a result of cAMP-binding. Dotted line indicates the end of the C-helix in the apo state. Residues used for FRET measurements are labeled yellow.

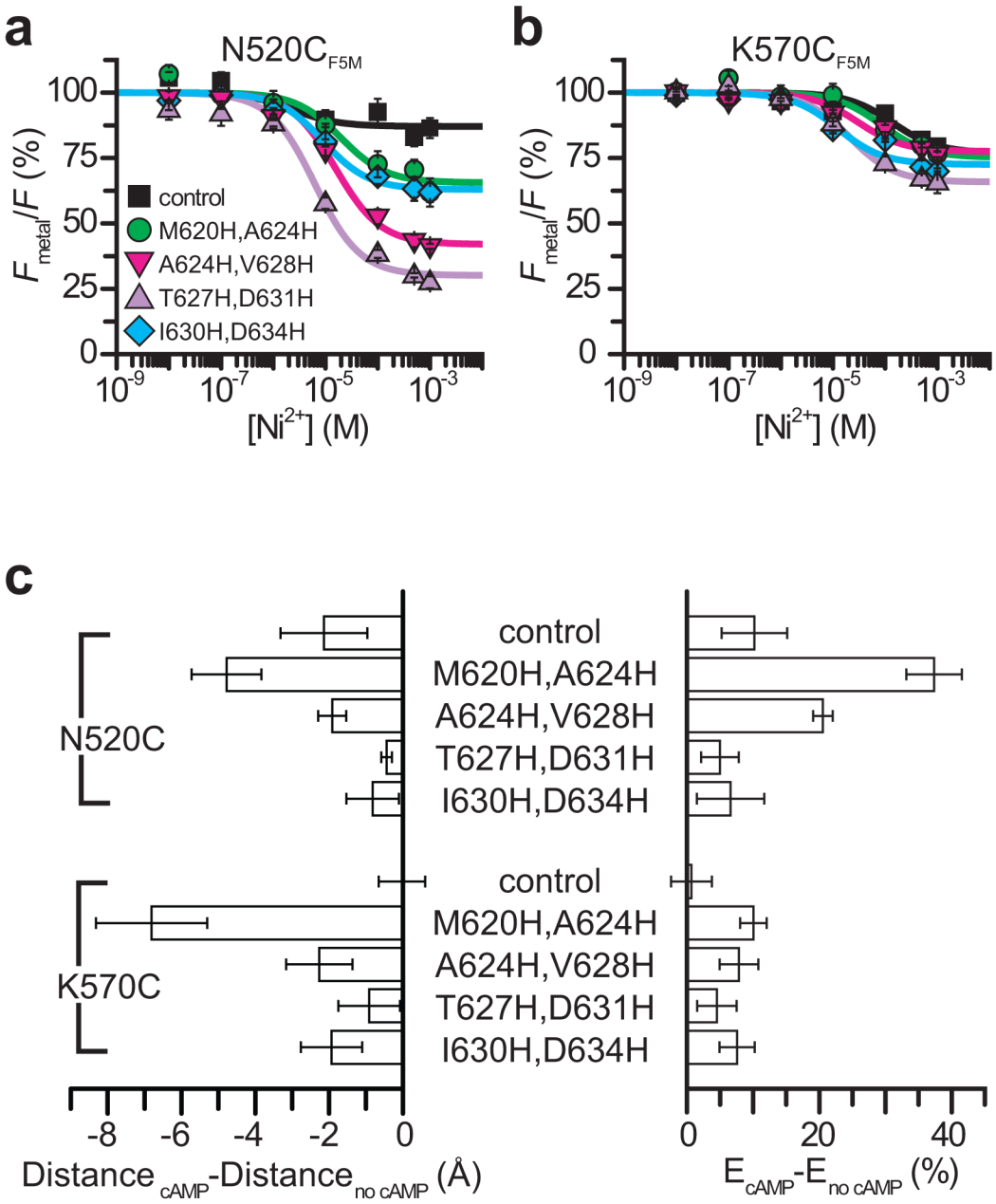

Figure 4.

Structural rearrangements in HCN2 determined with transition metal ion FRET. Ni^{2+}-dependent quenching of apo state HCN2 labeled with fluorescein-5-maleimide at N520C (**a**) and K570C (**b**) with Ni^{2+}-binding motifs in the C-helix. Control contains no introduced histidines. Fluorescence was normalized to the intensity before the addition of Ni^{2+} and fit by a single-site binding model (solid line). (**c**) Plot of FRET changes (right) and corresponding changes in distance (left) between the apo and holo states. Error bars are s.e.m. (n = 4–6).

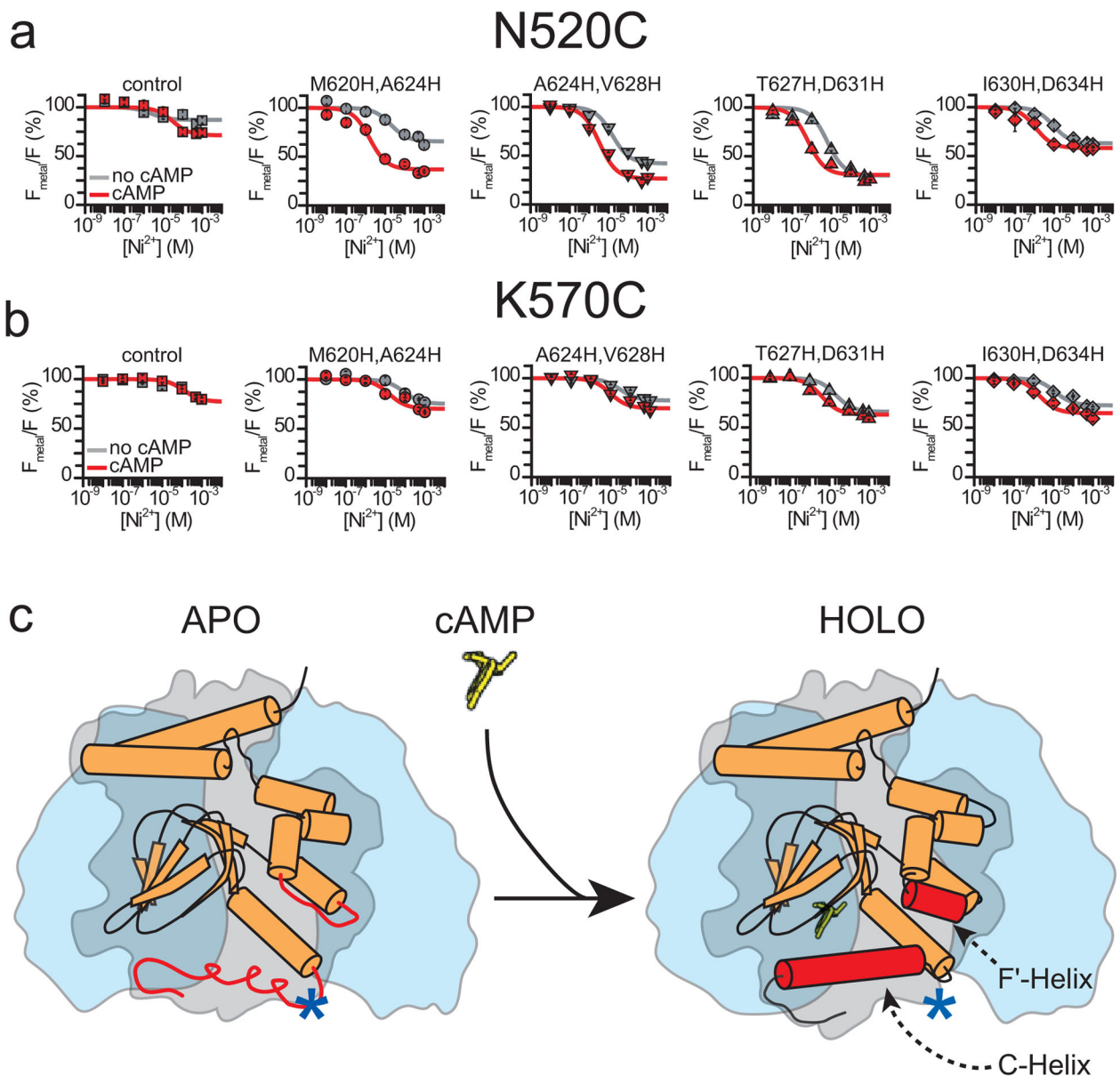

Figure 5.

The C-helix is stabilized during cAMP-binding. (**a,b**) Overlay of apo (grey) and holo (red) Ni^{2+}-quenching curves for (**a**) $N520C_{F5M}$ constructs and (**b**) $K570C_{F5M}$ constructs. (**c**) Current working hypothesis for the conformational rearrangements (red) that occur during cAMP-binding. Asterisk indicates the position of C-helix in the apo state.